Surg Endosc (2009) 23:1901–1907
DOI 10.1007/s00464-008-0263-8

NEW TECHNOLOGY

A new electrocautery pleural biopsy technique using an insulated-tip diathermic knife during semirigid pleuroscopy

Shinji Sasada · Kunimitsu Kawahara · Yoko Kusunoki · Norio Okamoto · Teruo Iwasaki · Hidekazu Suzuki · Masashi Kobayashi · Tomonori Hirashima · Kaoru Matsui · Mitsunori Ohta · Teruomi Miyazawa

Received: 10 August 2008 / Accepted: 15 November 2008 / Published online: 1 January 2009

Abstract
Background The biopsy size obtained with standard flexible forceps (SFF) during semirigid pleuroscopy is often insufficient for pathological examination. An insulated-tip diathermic knife (IT knife) allows safe resection of a larger lesion during gastrointestinal endoscopy. We sought to validate an electrocautery pleural biopsy technique using the IT knife during semirigid pleuroscopy. We compared the diagnosis of specimens obtained using the IT knife and SFF in 20 subjects with unexplained pleural effusion, and reviewed pleuroscopic parameters such as complications, procedure time, and diameter of the specimens.
Methods After injecting saline with lidocaine and epinephrine below the affected pleura, the lesion was incised in a circular shape with full thickness by manipulating the IT knife.
Results Diagnostic yields from specimens obtained with the IT knife and SFF were 85% (17 of 20 cases) and 60% (12 of 20 cases), respectively. The IT knife biopsy was superior to SFF in 8 of 20 patients (malignant pleural mesothelioma in three, nonspecific inflammation in two, metastatic breast cancer in one, and tuberculosis in one). These pleural lesions revealed thickened, smooth abnormal appearances. The overall diagnostic yield for both IT knife and SFF was 100%. Median time of the procedure, from first pleural injection to specimen removal, was 21 min (range 12–92 min), and median diameter of specimen was 13 mm (range 6–23 mm). There were no severe complications during the procedure.
Conclusions Electrocautery biopsy using the IT knife during semirigid pleuroscopy has great potential for diagnosing smooth abnormal pleura which are difficult to biopsy with SFF.

Keywords Insulated-tip diathermic knife · Electrocautery pleural biopsy · Semirigid pleuroscope · Smooth abnormal pleura · Full-thickness pleura

Abbreviations

IT knife	Insulated-tip diathermic knife
SFF	Standard flexible forceps
ESD	Endoscopic submucosal dissection
MPM	Malignant pleural mesothelioma
DDM	Desmoplastic malignant mesothelioma

Introduction

Obtaining an accurate diagnosis of pleural disease is one of the most common problems for a pulmonologist. After thoracocentesis and/or blind pleural biopsy, 25–40% of pleural abnormalities remain undiagnosed [1, 2]. Medical thoracoscopy is an invasive technique which should be used

S. Sasada (✉) · Y. Kusunoki · N. Okamoto · H. Suzuki · M. Kobayashi · T. Hirashima · K. Matsui
Department of Thoracic Malignancy, Osaka Prefectural Medical Center for Respiratory and Allergic Diseases, Osaka, Japan
e-mail: s-sasada@hbk.pref.osaka.jp

K. Kawahara
Department of Pathology, Osaka Prefectural Medical Center for Respiratory and Allergic Diseases, Osaka, Japan

T. Iwasaki · M. Ohta
Department of Pulmonary Surgery, Osaka Prefectural Medical Center for Respiratory and Allergic Diseases, Osaka, Japan

T. Miyazawa
Department of Pulmonology, St. Marianna University School of Medicine, Kanagawa, Japan

when other more simple methods fail; it involves examining the pleural space under local anesthesia [3, 4]. It enables a positive diagnosis in >90% of pleural effusions [5, 6].

Some investigators use a fiber-optic bronchoscope [7–10], but most prefer a rigid thoracoscope because it allows better observation of the pleural cavity and larger biopsies [11–13]. On the other hand, in the UK, medical thoracoscopy was not widespread because most pulmonologists were unfamiliar with the usage of the more commonly used rigid thoracoscope [14]. The semirigid pleuroscope was developed in an attempt to combine the best features of the flexible and rigid instruments [15]. This instrument is easy to handle and covers a wider field because the handle is similar in design to a standard flexible bronchoscope [16–18]. However, the biopsy size obtained from a semirigid pleuroscope using flexible forceps is smaller than that from a rigid instrument [18, 19], which directly impacts on diagnostic results. In particular, the diagnosis of mesothelioma was shown to be extremely difficult with small biopsies because it can demonstrate various misleading and histopathological pitfalls [20]. The tumor has a varied and deceptive appearance in a high percentage of cases and may resemble benign pleural or metastatic lesions [20].

In 1994, Japanese gastrointestinal endoscopists developed a special endoscope knife, called the insulated-tip diathermic knife (IT knife) [21]. The IT knife allows for safe resection of a larger gastric lesion in a single piece. The average rate of complete resection has increased to more than 90% and histological evaluation has become easier. This technique is called endoscopic submucosal dissection (ESD) and many patients with early gastric carcinomas have recently been treated with ESD [22–24].

The purpose of this study was to investigate the potential use of the IT knife as a new pleural biopsy devise in unexplained pleural effusions; to compare its diagnostic efficiency with that of standard flexible forceps (SFF) biopsy; and to review pleuroscopic parameters such as complications, procedure time, and size of specimens.

Materials and methods

This study was a single-center prospective study which included referred patients with a pleural effusion and a negative or unsuccessful blind pleural fluid aspirate or biopsy. All patients underwent a computed tomography (CT) scan of the thorax prior to participation. Patients with "highly suspicious" pleural fluid cytology were excluded unless the cytological diagnosis was inconsistent with clinical features and CT findings. Patients with apparent pleural nodules or masses on CT or direct vision during pleuroscopy were also excluded. Cases of cardiopulmonary dysfunction, coagulation disorder, and severe pleural adhesion without free space in the chest cavity were considered contraindications. This study was approved by the review boards of the participating institutions. All patients were given a detailed description of the examination and were informed that a new technique was being evaluated. Informed consent was obtained from all patients.

The instrument employed was a semirigid pleuroscope (LTF-240; Olympus, Tokyo, Japan) with controls similar to that of a flexible fiberoptic bronchoscope. The total length of the instrument is 52 cm, with the insertion portion being 27 cm long. Of this, the proximal 22 cm are rigid and the distal 5 cm are flexible. The external diameter of the insertion portion is 7 mm. The tip is bendable in one plane, with an upward angulation of 130° and downward angulation of 130°. The 2.8-mm inner working channel accommodates the biopsy forceps and other instruments.

The insulated-tip diathermic knife (IT knife; Olympus, Tokyo, Japan) is designed specifically to minimize the risk of gastric wall perforation and consists of a conventional diathermic needle knife with a ceramic ball at the tip (Fig. 1). The outer diameter of the IT knife and the length of the needle knife are 2.2 mm and 4 mm, respectively. The IT knife is a disposable product with a preferred working channel diameter of at least 2.8 mm. In order to treat early gastric carcinoma endoscopically, the IT knife is manipulated as follows. First, dotted marks are made along the outline of the localized gastric lesion. Second, an injection of saline containing epinephrine is administered until the gastric mucosa around the lesion becomes elevated. Finally, all layers of the gastric mucosa are incised and resected with the IT knife.

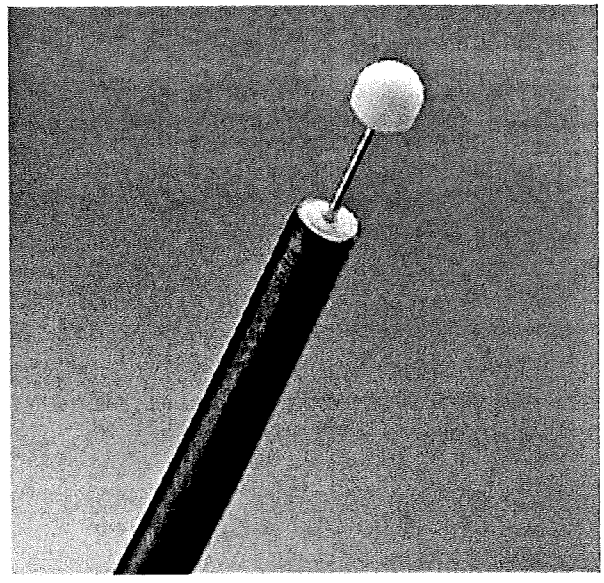

Fig. 1 Specifications for the insulated-tip diathermic knife, consisting of a conventional diathermic needle knife with a ceramic ball at the tip

Procedure

All procedures were performed by two operators in the endoscopy suite of the present authors' institution (Osaka Prefectural Medical Center for Respiratory and Allergic Diseases, Osaka, Japan). A single puncture technique was used. The lateral decubitus position was employed, with the diseased side facing upward. The semirigid pleuroscope was then inserted and, following drainage of all fluid to dryness, the pleural surfaces were inspected. Upon confirming the location of the pleural lesion, a SFF (FB-55CR-1; Olympus) biopsy was taken. Following this, a subpleural injection of saline containing 0.5% lidocaine and 0.005% epinephrine was administered using an injection needle (NM-9L-1; Olympus) until the affected pleura was raised. An initial puncture was made with coagulation forceps (FD-6C-1; Olympus). After a pinhole was made, the tip of the IT knife was inserted into the hole. The affected pleura was incised in a circular shape with full thickness by manipulating the IT knife with the combination output of cutting and coagulation current at 30–40 W (ICC200; ERBE, Tubringen, Germany). The incised pleura was carefully removed with SFF. Thoracoscopic specimens obtained using the IT knife and SFF were fixed in formalin.

Endoscopic parameters and pathological definitions

We recorded any complications that were specific to the electrocautery biopsy using the IT knife. Procedure time was measured from first subpleural injection to specimen removal. During the procedure, the thickness of the parietal pleura was endoscopically measured and graded into three levels as follows: slight (2 mm or less), moderate (2–4 mm), or severe (4 mm or more). These values were measured at the punctured hole by matching with the IT knife tip insertion depth, which we considered a measure of pleural thickness. Following the procedure, the diameter of the obtained circular specimens was measured using a ruler.

The pathological findings were independently obtained by two pathologists (K.K. and T.N.) and compared with

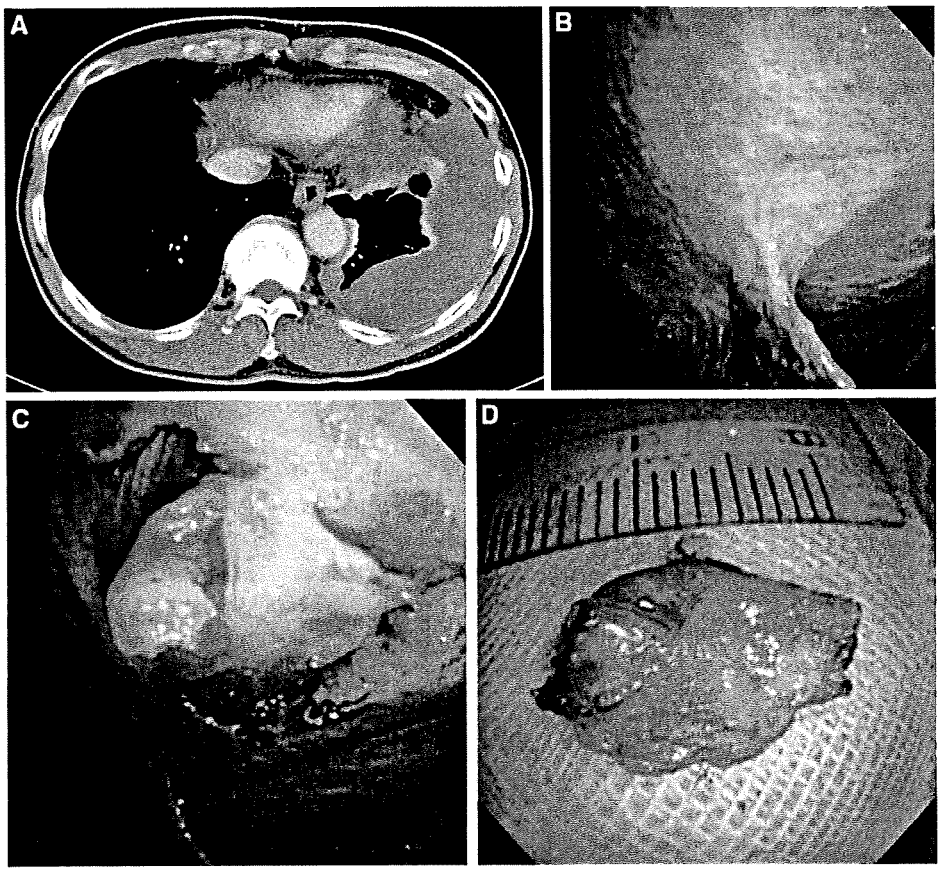

Fig. 2 Electrocautery pleural biopsy using IT knife in case 3. **A** Chest computed tomography indicated pleural effusion and thickened parietal pleura on the left side. **B** Whitish, thickened parietal pleura with smooth pleural surface observed endoscopically. **C** After an initial puncture was made with coagulation forceps, the tip of the IT knife was inserted into the hole (not shown). The affected pleura was incised in a circular shape with full-thickness. **D** The circular obtained specimen; largest diameter is 14 mm

those obtained using SFF. If the specimens revealed specific pathological findings for definitive diagnosis, we judged it as successful. On the other hand, the following conditions were judged as failures: no specimen, minuscule specimen without specific findings, and no specific pathologic findings for definitive diagnosis.

Results

A total of 20 patients with unexplained pleural effusion participated in this study during January 2006 and December 2007 and underwent medical thoracoscopy using a semirigid pleuroscope (Fig. 2). The patients were 14 men and 6 women, with median age of 69 years (Table 1). The lesion sides were predominantly on the right (14 of 20 patients). Thoracoscopic views indicated that all patients had thickened pleura with additional changes, such as fibrous adhesion, hypervascularization, small nodules, granulation, and diffuse dense fibrosis. The distribution of the degree of pleural thickness was as follows: 6 slight (30%), 10 moderate (50%), and 4 severe (20%). Table 2 shows the pleuroscopic parameters. The median time of the procedure, from first pleural injection to specimen removal, was 21 min (range 12–92 min), and the median of the largest diameter of specimens was 13 mm (range 6–23 mm). One patient experienced mild chest pain, but there were no severe complications during the procedure in all patients. Although mild bleeding was observed in almost all cases, we did not consider these events as specific complications.

Table 3 shows the diagnostic comparisons between specimens obtained using the IT knife and SFF. All patients successfully underwent electrocautery pleural biopsy with the IT knife except for one patient with sarcomatous mesothelioma (case 6). Diagnostic yields with specimens obtained using the IT knife and SFF were 85% (17 of 20 cases) and 60% (12 of 20 cases), respectively. The IT knife biopsy was superior to SFF in 8 of 20 patients [malignant pleural mesothelioma (MPM) in three, nonspecific inflammation in two, metastatic breast cancer in one, and tuberculosis in one]. These lesions have thickened, smooth abnormal appearance. Two patients with lung adenocarcinoma (cases 7 and 8) and case 6 could not be diagnosed with the specimen obtained using the IT knife, but random biopsy specimens obtained by SFF were successful in diagnosis. Seven patients with lesions determined to be nonspecific inflammation did not have a recurrence during the subsequent observation period, which is consistent with the clinical characteristics of

Table 1 Clinical characteristics and pleuroscopic findings during electrocautery biopsy using IT knife

Patient no.	Age (years)/sex/side of pleural effusion	Pleuroscopic findings, measured value of the thickness of the parietal pleura
1	72/F/Rt	Moderate thickened pleura with fibrinous adhesion, patchy pleural plaque, and small nodules
2	65/M/Lt	Slight thickened pleura with hypervascularization, and patchy pleural plaque
3	59/M/Lt	Severe thickened pleura with diffuse dense fibrosis
4	64/M/Rt	Severe thickened pleura with diffuse dense fibrosis, and fibrinous adhesion
5	74/F/Lt	Moderate thickened pleura
6	63/M/Rt	Severe thickened pleura with fibrinous adhesion
7	76/M/Rt	Moderate thickened pleura with diffuse dense fibrosis, and fibrinous adhesion
8	79/M/Rt	Moderate thickened pleura, and small nodules
9	66/F/Rt	Slight thickened pleura with fine granulation, and a small number of pleural plaque
10	79/M/Rt	Moderate thickened pleura with hypervascularization, edema, and a little nodules
11	69/F/Rt	Slight thickened pleura with whitish fine granulation, and edema
12	69/M/Rt	Slight thickened pleura
13	55/M/Lt	Moderate thickened pleura with fibrinous adhesion
14	53/F/Lt	Moderate thickened pleura with fibrinous adhesion
15	69/F/Lt	Slight thickened pleura with hypervascularization
16	75/M/Rt	Moderate thickened pleura with diffuse dense fibrosis
17	79/M/Rt	Severe thickened pleura with diffuse dense fibrosis, and fibrinous adhesion
18	73/M/Rt	Moderate thickened pleura with diffuse dense fibrosis, and patchy plaque
19	59/M/Rt	Moderate thickened pleura with diffuse dense fibrosis
20	77/M/Rt	Slight thickened pleura with diffuse dense fibrosis

M, male; *F*, female; *Rt*, right; *Lt*, left

Table 2 Pleuroscopic parameters during electrocautery biopsy using IT knife

Patient no.	Time[a] (min)	Diameter of IT knife specimen (mm)	Complications[b]
1	21	13	No
2	23	23	No
3	23	14	No
4	22	15	No
5	92	6	No
6[c]	No data	No data	No data
7	12	18	Chest pain
8	20	13	No
9	26	10	No
10	31	22	No
11	20	8	No
12	15	15	No
13	32	14	No
14	27	14	No
15	40	10	No
16	32	9	No
17	15	6	No
18	19	12	No
19	20	16	No
20	14	15	No

[a] Time was measured from first subpleural injection to specimen removal

[b] Mild bleeding is not decided as a specific complication

[c] Sufficient materials could not be obtained with IT knife

The median time of the procedure was 21 min (range 12–92 min). The median of the largest diameter of specimens was 13 mm (range 6–23 mm). There were no severe complications during the procedure in all patients

inflammation. Overall diagnostic yield for both the IT knife and SFF was 100%.

Eight lesions diagnosed using only the IT knife were unattainable using SFF, and the degree of thickness were as follows: three slight, three moderate, and two severe. There was no relationship between degree of thickness and difficulty in performing the SFF biopsy.

Discussion

Pleuroscopy is recommended to diagnose pleural disease because it is superior to blind pleural biopsy, but there are no clear criteria as to the best choice of equipment. Semirigid pleuroscopy under local anesthesia has been performed because it is a simple method and costs little compared with video-assisted thoracoscopy under general anesthesia. The choice of equipment often differs by the medical care circumstances of institutions and by country, such as the availability of a rigid telescope or a semirigid pleuroscope. Some pulmonologists prefer the semirigid pleuroscope because the handle is similar in shape to the bronchoscope, but it is unable to obtain sufficiently sized specimens because its operating channel and exclusive forceps are too small. Since it is not possible to perform careful pathological analyses with small specimens, including immunohistochemical examination, diagnosis may not be possible [25–27]. In this study, we determined that electrocautery biopsy using the IT knife can increase diagnostic ability in patients with unexplained pleural effusion. The successful IT knife cases mainly involved thickened pleura with smooth abnormal appearances. In this study, we succeeded in hollowing out the pleural lesions by electrocautery biopsy using the IT knife, and were able to safely and effectively obtain a large amount of tissue, as recommended for diagnostic purposes.

In order to obtain an accurate biopsy of MPM, including the thickening pattern, it is important to obtain multiple, large biopsy samples (10 mm in length and 5 mm in width) using a rigid thoracoscope [19]. In the present study, three of six MPMs (50%) were successfully diagnosed by the large circular specimens obtained using the IT knife. Desmoplastic malignant mesothelioma (DMM) is a rare variant of MPM that exhibits a storiform collagen pattern [28]. We believe that biopsy specimens of adequate size and full thickness should be obtained to improve the diagnostic yield even in DMM [29]. In our cases, the original pleural structure was maintained within the full-thickness biopsy specimens. The electrocautery biopsy specimens obtained using the IT knife allowed us to obtain an adequate amount of information, which was not possible with flexible forceps [30].

In the present study, we also assessed the association between pleural thickness and difficulty in biopsy. In our findings, eight pleural lesions with unattainable status by SFF biopsy did not all display severe thickening (two of

Table 3 Diagnostic comparison between specimens obtained with the IT knife and standard flexible forceps

Patient no.	Definitive diagnosis	Diagnosis with IT knife	Diagnosis with SFF	Overall diagnosis
1	Epithelial mesothelioma	Success	Success	Success
2	Epithelial mesothelioma	Success	Failure	Success
3	Epithelial mesothelioma	Success	Failure	Success
4	Desmoplastic mesothelioma	Success	Failure	Success
5	Sarcomatous mesothelioma	Success	Success	Success
6	Sarcomatous mesothelioma	Failure[a]	Success	Success
7	Lung adenocarcinoma	Failure	Success	Success
8	Lung adenocarcinoma	Failure	Success	Success
9	Metastatic breast cancer	Success	Failure	Success
10	Malignant lymphoma	Success	Success	Success
11	Tuberculosis	Success	Success	Success
12	Tuberculosis	Success	Success	Success
13	Tuberculosis	Success	Failure	Success
14	Nonspecific inflammation	Success	Success	Success
15	Nonspecific inflammation	Success	Success	Success
16	Nonspecific inflammation	Success	Success	Success
17	Nonspecific inflammation	Success	Success	Success
18	Nonspecific inflammation	Success	Failure	Success
19	Nonspecific inflammation	Success	Failure	Success
20	Nonspecific inflammation	Success	Failure	Success
Diagnostic yields		85% (17/20)	60% (12/20)	100% (20/20)

SFF, standard flexible forceps

[a] Sufficient materials could not be obtained with IT knife

eight lesions). Consequently, it appears that there is no clear association between diagnostic difficulty and pleural thickness.

Pleural hemorrhage and pain were considered as potential serious complications with our technique. We injected epinephrine and lidocaine just above the endothoracic fascia, thereby potentially reducing pleural hemorrhage and pain. For safety, we carefully sought only completely raised pleural areas. We did not experience any major specific complications with our new technique. In addition, this technique could be performed in about 20 min, from the first subpleural injection to specimen removal, which is considered acceptable for a full examination. However, this procedure is not always possible in the pleural cavity without a surgical procedure; for example, to access an apex, physicians may have to manipulate from a distressed, tangential view and may not be able to perform biopsies. An optimal area for biopsy is the caudal lateral pleura.

In conclusion, we found that electrocautery biopsy using the IT knife during semirigid pleuroscopy has great potential for diagnosing smooth abnormal pleura which are difficult to biopsy using SFF. This technique may aid pulmonologists in diagnosing a smooth pleural lesion even when biopsy is difficult with rigid instruments.

Acknowledgements The authors would like to thank the many nurses and physicians who participated in the care of patients in the study; Dr. Tomoki Michida for providing technical advice on using the IT knife; Dr. Atsuko Ishida for supporting the study; and Dr. Teruaki Nagano for supporting the pathologic examinations. This work was supported by grants from the Osaka Medical Research Foundation for Incurable Diseases.

References

1. Poe RH, Israel RH, Utell MJ et al (1984) Sensitivity, specificity, and predictive values of closed pleural biopsy. Arch Intern Med 144:325–328
2. Prakash UBS, Relman H (1985) Comparison of needle biopsy with cytologic analysis for the evaluation of pleural effusion: analysis of 414 cases. Mayo Clin Proc 60:158–164
3. McLean AN, Stephen RB, Lawrence GM, Andrew JP (1998) Investigation of pleural effusion: an evaluation of the new Olympus LTF semiflexible thoracofiberscope and comparison with abram's needle knife. Chest 114:150–153
4. Boutin C, Viallat JR, Cargnino P, Farisse P (1981) Thoracoscopy in malignant pleural effusions. Am Rev Respir Dis 124:588–592
5. Canto A, Blasco E, Casillas M et al (1977) Thoracoscopy in the diagnosis of pleural effusion. Thorax 32:550–554
6. Weissberg D, Kaufmann M (1980) Diagnostic and therapeutic pleuroscopy. Experience with 27 patients. Chest 78:732–735
7. Senno A, Moallem S, Quijano ER et al (1974) Thoracoscopy with the fiberoptic bronchoscope. A simple method in diagnosing pleuropulmonary diseases. J Thorac Cardiovasc Surg 67:601–611

8. Gunnels JJ (1978) Perplexing pleural effusion. Chest 74:390–393
9. Ben Isaac FE, Simmons DH (1975) Flexible fiberoptic pleuroscopy: pleural and lung biopsy. Chest 67:573–576
10. Kerby GR, Pierce G, Ruth WE (1975) Clinical experience with pleuroscopy utilizing the bronchofiberscope. Ann Otol 84:602–606
11. Oldenburg FA, Newhouse MT (1979) Thoracoscopy. A safe, accurate diagnostic procedure using the rigid thoracoscope and local anesthesia. Chest 75:45–50
12. Ash SR, Manfredi F (1974) Directed biopsy using a small endoscope. Thoracoscopy and peritoneoscopy simplified. N Engl J Med 291:1398–1399
13. Boushy SF, North LB, Helgason AH (1974) Thoracoscopy: technique and results in eighteen patients with pleural effusion. Chest 4:386–389
14. Mathur PN (2004) Pleuroscopy: a window to the pleura. J Bronchol 11:147–149
15. Ernst A, Hersh CP, Thurer R et al (2002) A novel instrument for the evaluation of the pleural space. Chest 122:1530–1534
16. Sakuraba M, Masuda K, Hebisawa A, Sagara Y, Komatsu H (2006) Diagnostic value of thoracoscopic pleural biopsy for pleurisy under local anesthesia. ANZ J Surg 76:722–724
17. Ernst A, Hersh CP, Herth F, Thurer R, LoCicero J III, Beamis J, Mathur P (2002) A novel instrument for the evaluation of the pleural space: an experience in 34 patients. Chest 122:1530–1534
18. Munavvar M, Khan MAI, Edwards J, Waqaruddin Z, Mills J (2007) The autoclavable semirigid thoracoscope: the way forward in pleural diseases? Eur Respir J 29:571–574
19. Boutin C, Viallat JR, Aelony Y (1993) Thoracoscopy in pleural mesothelioma: a prospective study of 188 consecutive patients. Part 1: diagnosis. Cancer 72:389–393
20. Greillier L, Cavailles A, Fraticelli A et al (2007) Accuracy of pleural biopsy using thoracoscopy for the diagnosis of histologic subtype in patients with malignant pleural mesothelioma. Cancer 110:2248–2252
21. Ono H, Kondo H, Gotoda T, Shirao K, Yamaguchi H, Saito D, Hosokawa K, Shimoda T, Yoshida S (2001) Endoscopic mucosal resection for treatment of early gastric cancer. Gut 48:225–229
22. Hirasaki S, Tanimizu M, Moriwaki T, Hyodo I, Shinji T, Koide N, Shiratori Y (2004) Efficacy of clinical pathway for the management of mucosal gastric carcinoma treated with endoscopic submucosal dissection using an insulated-tip diathermic knife. Int Med 43:1120–1125
23. Gotoda T (2005) A large endoscopic resection by endoscopic submucosal dissection procedure for early gastric cancer. Clin Gastroenterol Hepatol 3:S71–S73
24. Miyazaki S, Gunji Y, Aoki T, Nakajima K, Nabeya Y, Hayashi H, Shimada H, Uesato M, Hirayama N, Karube T, Akai T, Nikaidou T, Kouzu T, Ochiai T (2005) High en-bloc resection rate achieved by endoscopic mucosal resection with IT-knife for early gastric cancer. Hepato-Gastroenterology 52:954–958
25. Lee P, Colt HG (2007) State of the art: pleuroscopy. J Thorac Oncol 2:663–670
26. Philip TC, Andrew C (2005) Differential diagnosis of benign and malignant mesothelial proliferations on pleural biopsies. Arch Pathol Lab Med 129:1421–1427
27. Butnor KJ (2006) My approach to the diagnosis of mesothelial lesions. J Clin Pathol 59:564–574
28. Wilson GE, Hasleton PS, Chatterjee AK (1992) Desmoplastic malignant mesothelioma: a review of 17 cases. J Clin Pathol 45:295–298
29. Sasada S, Kawahara K, Iwasaki T, Hirashima T, Miyazawa T (2008) An electrocautery pleural biopsy for the diagnosis of desmoplastic malignant mesothelioma during semirigid thoracoscopy. J Thorac Oncol 3:803–804
30. Kawahara K, Sasada S, Nagano T, Suzuki H, Kobayashi M, Matsui K, Takata K, Yoshino T, Michida T, Iwasaki T (2008) Pleural MALT lymphoma diagnosed on thoracoscopic resection under local anesthesia using an insulation-tipped diathermic knife. Pathol Int 58:253–256

EUROPEAN JOURNAL OF CANCER 45 (2009) 2132–2137

available at www.sciencedirect.com

ScienceDirect

journal homepage: www.ejconline.com

Phase I/II study of S-1 plus carboplatin in patients with advanced non-small cell lung cancer

Kenji Tamura[a,b,*], *Isamu Okamoto*[b], *Tomohiro Ozaki*[c], *Tatsuhiko Kashii*[d], *Koji Takeda*[d], *Masashi Kobayashi*[e], *Kaoru Matsui*[e], *Takashi Shibata*[a], *Takayasu Kurata*[f], *Kazuhiko Nakagawa*[b], *Masahiro Fukuoka*[g]

[a]Outpatients Treatment Center, National Cancer Center Hospital, 5-1-1, Tsukiji, Chuo-ku, Tokyo, Japan
[b]Department of Medical Oncology, Kinki University School of Medicine, 377-2, Ohno-higashi, Sayama, Osaka, Japan
[c]Department of Medical Oncology, Kinki University School of Medicine, Nara Hospital, 1248-1, Otoda, Ikoma, Nara, Japan
[d]Department of Clinical Oncology, Osaka City General Hospital, 2-13-22, Miyakojima-hondori, Miyakojima, Osaka, Japan
[e]Department of Thoracic Malignancy, Osaka Prefectural Medical Center for Respiratory and Allergic Diseases, 3-7-1, Habikino, Habikino, Osaka, Japan
[f]Cancer Chemotherapy Center, Osaka Medical College, 2-7, Daigaku, Takatsuki, Osaka, Japan
[g]Department of Medical Oncology, Kinki University School of Medicine, Sakai Hospital, 2-7-1, Harayamadai, Minami-ku, Sakai, Osaka, Japan

ARTICLE INFO

Article history:
Received 24 February 2009
Accepted 1 April 2009
Available online 4 May 2009

Keywords:
Non-small cell lung cancer (NSCLC)
S-1
Carboplatin
Phase I/II study
Chemotherapy

ABSTRACT

The objective of this phase I/II study was to determine the recommended dose (RD) of S-1 and carboplatin (CBDCA), and to evaluate the efficacy and safety of this combination in the treatment of patients with advanced non-small cell lung cancer (NSCLC). Chemotherapy-naïve patients were treated with S-1 given orally on days 1–14, and CBDCA infused intravenously on day 1, repeated every 3 weeks. RD was AUC5 of CBDCA and 80 mg/m^2 of S-1. Nineteen patients were treated at the RD. The overall response was 30.8% (95% confidence interval: 17.1–58.3%). The response rate in the RD was 36.8% (95% CI: 16.3–61.6%). The median overall survival time was 11.1 months (95% CI: 8.1–15.3 months) and the median progression-free survival time was 5.0 months (95% CI: 3.6–6.0 months). Major grades 3–4 toxicities were thrombocytopaenia (47%), anaemia (26%) and infection (16%). This is the first report to show promising activity of this combination in phase II, including survival data and manageable toxicity, especially in outpatients receiving treatment for advanced NSCLC.

1. Introduction

Lung cancer is a leading cause of cancer mortality in many countries.[1] Combination chemotherapy with platinum agents and new-generation non-platinum anti-tumour agents, for example, paclitaxel, docetaxel[2], vinorelbine[3] and gemcitabine[4], has been regarded as the standard treatment for advanced stage non-small cell lung cancer (NSCLC)[5], although outcomes are far from acceptable.

S-1, a fourth-generation oral fluoropyrimidine, is a formulation of tegafur (FT), 5-chloro-2,4-dihydroxypyridine (CDHP) and potassium oxonate (Oxo) at a molar ratio of 1:0.4:1.[6] FT is the prodrug for cytotoxic fluorouracil (FU) and CDHP prevents its degradation. CDHP is a potent and competitive

* *Corresponding author:* Outpatients Treatment Center, National Cancer Center Hospital, 5-1-1, Tsukiji, Chuo-ku, Tokyo, Japan. Tel.: +81 3 35422511; fax: +81 3 35423815.
E-mail address: ketamura@ncc.go.jp (K. Tamura).
0959-8049/$ - see front matter © 2009 Elsevier Ltd. All rights reserved.
doi:10.1016/j.ejca.2009.04.003

inhibitor of dihydropyrimidine dehydrogenase, which reduces the degradation of FU and allows efficacious concentrations to enter the anabolic pathway.[7] Oral S-1 administration can generate a higher concentration of 5-FU than protracted intravenous injection of 5-FU, without increasing the incidence of adverse events affecting the gastrointestinal tract.[8]

In a phase II study, which involved monotherapy with S-1 at 80 mg/m^2/day for 28 d followed by a 2-week rest period in chemotherapy-naïve advanced NSCLC patients, the overall response rate was 22%, and the median survival time (MST) was 10.2 months.[9] Combination chemotherapy with cisplatin (60 mg/m^2 on day 8) and S-1 (80 mg/m^2, from days 1 to 21) every 5 weeks resulted in a response rate of 47% and a MST of 11.0 months.[10] Although cisplatin is a basic drug for advanced NSCLC, the relative dose intensity of cisplatin with this regimen was 12 mg/week, considerably lower than the standard (23–27 mg/week). Furthermore, intravenous injection of cisplatin requires hospitalisation for hydration, i.e. to prevent renal toxicity, which negates the advantage and convenience of S-1 as an orally administrated drug allowing outpatient treatment. Carboplatin-based regimens that are less toxic, convenient and capable of being administered on an outpatient basis, thereby maintaining the patient's quality of life, need to be developed. However, there were no confirmed data about fix doses of combination of S-1 plus carboplatin in advanced stage NSCLC as first-line setting.

We conducted the present phase I/II study with oral administration of S-1 for 14 consecutive days and carboplatin on day 1 every 3 weeks in chemotherapy-naïve patients with advanced NSCLC, and determined the efficacy and safety of this regimen.

2. Patients and methods

2.1. Objective

The objective of this study was to determine the maximum tolerable dose (MTD), the toxicity profile, the RD and the setting of dose-limiting toxicity (DLT), and to evaluate efficacy and safety, in chemotherapy-naïve patients with advanced NSCLC.

2.2. Eligibility criteria

Chemotherapy-naïve patients with histologically or cytologically confirmed stage IIIB NSCLC, diagnosed as having no treatment indications for thoracic irradiation, or stage IV, were eligible. Cases with recurrent disease after curative surgery were also eligible. Adjuvant chemotherapy was not counted as one regimen. At least one measurable lesion was necessary as part of the phase II trial. Other eligibility criteria included being 20 to 75 years of age, Eastern Cooperative Oncology Group performance status (PS) of 0–1, adequate organ function (white blood cell count (WBC) $\geqslant$ 4000/μL, platelet count $\geqslant$ 100,000/μL, haemoglobin concentration $\geqslant$ 9.0 g/dL, serum bilirubin $\leqslant$ 2.0 mg/dL, AST and ALT $\leqslant$ 100 IU/L, serum creatinine $\leqslant$ institutional upper limit of normal range; $PaO_2 \geqslant 60$ mmHg). The main exclusion criteria were: active concomitant malignancy, congestive heart failure, uncontrolled angina pectoris, arrhythmia, hypertension, uncontrolled diabetes, symptomatic infectious disease, severe haemorrhage/bleeding, pulmonary fibrosis or interstitial pneumonia, obstructive bowel disease or severe diarrhoea, symptomatic peripheral effusion, cardiac effusion and ascites, symptomatic brain metastasis and pregnancy or breast feeding. This study was approved by the institutional review board at each participating centre. All patients gave written informed consent prior to registration.

2.3. Treatment plan

Patients received variable doses of intravenous carboplatin administered as a 60-min infusion on day 1 and variable doses of oral S-1 administered on days 1–14, every 3 weeks. Carboplatin doses were determined using serum creatinine values and the Calvert formula[11] based on the targeted area under the time-concentration curve (AUC). Patients were treated for at least four cycles unless disease progression or unacceptable toxicity was observed. S-1 administration was interrupted when grade 4 neutropaenia, grade 4 thrombocytopaenia or grade 3 or more severe non-haematological toxicity developed, and was reinitiated when neutrophil counts $\geqq$ 1000//μL, platelet counts $\geqq$ 75000//μL and non-haematological toxicity of grade 2 or less were observed. Subsequent chemotherapy was initiated when the leukocyte counts $\geqq$ 4000//μL, platelet counts $\geqslant$ 100,000/μL, haemoglobin concentration $\geqslant$ 9.0 g/dL, serum creatinine $\leqslant$ 1.5 g/dL, $PaO_2 \geqslant 60$ mmHg and non-haematological toxicity of grade 2 or less were observed.

2.4. Dose escalation

The dose escalation schedule is shown in Table 2. At least three patients were enrolled at each dose level. Initially, three treated patients were treated at dose level 1 and no intra-individual dose escalation was performed. If one DLT was observed in the first three patients, three more patients were enrolled at this dose level, and dose escalation continued to the next level if fewer that three of the six patients experienced DLT during the first cycle. The MTD was defined as the level prior to that at which DLT was observed in two of three or in three of six patients during the first cycle. If all three patients experienced a DLT at level 1, a dose reduction to level 0 was planned. DLTs were defined as: (a) grade 4 neutropaenia lasting 5 d or longer; (b) febrile neutropaenia (grade 3 or 4 neutropaenia with fever (>38.5 °C)); (c) grade 4 thrombocytopaenia; (d) grade 3 or 4 non-haematological toxicity except for nausea, vomiting, anorexia, general fatigue and alopecia; (e) any unresolved toxicity, requiring a delay in administration of the second course exceeding 14 d and (f) inability to administer S-1 for more than seven consecutive days during treatment. Prophylactic administration of granulocyte colony-stimulating factor (G-CSF) was not allowed at any time during this study.

2.5. Patient evaluation

Haematological and biochemical tests, PS and clinical symptoms were monitored at least once a week. Toxicities were evaluated according to the National Cancer Institute (NCI) Common Toxicity Criteria, version 3.0 (NCI CTCAE V 3.0;

Table 1 – Patient characteristics.

Number of patients	28
Age, years; median (range) 6 (37–73)	66 (37–73)
Gender	
Male	20
Female	8
Performance status (ECOG)	
0	7
1	21
UICC-Stage	
IIIB	4
IV	24
Histology	
Adenocarcinoma	20
Squamous cell carcinoma	4
Large cell carcinoma	3
Others	1
Prior treatment	
Surgery	
Excision of cranial metastasis	2
Radiation therapy	
Whole brain radiotherapy	3
Palliative radiotherapy	1

available from http://ctep.info.nih.gov/CTC3/ctc.html). Tumour response was assessed according to the Response Evaluation Criteria in Solid Tumours (RECIST).[12] Time to progression and overall survival were estimated using the Kaplan–Meier method.

2.6. Statistical analyses

A one-stage design using the binominal probability was used to determine the sample size. Assuming that a response rate of 30% would indicate potential usefulness, whereas a rate of 10% would be the lower limit of interest, and with $\alpha = .05$ (one-side) and $\beta = .20$, the estimated accrual number was 24 patients.

3. Results

3.1. Patient characteristics

Between June 2005 and February 2007, 28 patients were enrolled in this study and their characteristics are listed in Table 1. Median age was 62 years (range 37–73). Twenty patients were male and six were female. All patients had good PS (ECOG 0 or 1). Four patients had stage IIIB, and were considered to have no indications for thoracic irradiation, and 24 patients had stage IV. The predominant histological type was adenocarcinoma (71%). Two patients had undergone surgical removal of brain metastases and four patients had received radiation therapy for brain metastasis or pain control.

3.2. Toxicities and dose escalation

Three patients each were entered at levels 1 and 2, and no DLTs were observed (Table 2). The next cohort of three patients received dose level 3 and one patient experienced a delay of more than 2 weeks (38 d) from the starting date of the second course due to thrombocytopaenia. Therefore, one of the first three patients had experienced DLT, when this group was expanded to six patients. Two of three additional patients also experienced delays of more than 2 weeks in starting the second course. One patient could not start the second course after a delay of more than 40 d due to thrombocytopaenia. Another patient started the second course after a delay of more than 18 d due to leucopaenia; thus, three of six patients had DLTs at level 3. Therefore, level 2 was regarded as the RD for the phase II study.

An additional 16 patients were added to level 2, such that 19 patients in total received AUC5 carboplatin on day 1 and 80 mg/m^2 S-1 on days 1–14, every 3 weeks. The median number of treatment cycles was 4 (range 2–6). The major adverse events during the entire treatment period are shown in Table 3. The haematological adverse events reaching grades 3–4 were anaemia (26%), thrombocytopaenia (47%) and leukocytopaenia (10.5%). Of these events, grade 4 thrombocytopaenia and anaemia were observed in one patient, and grade 4 thrombocytopaenia in another. Grades 3–4 non-haematological toxicities were gastritis, anorexia, nausea/vomiting, fatigue and elevation of total bilirubin in one patient each. Grade 3 infection (16%) was observed in three patients (two pneumonias; one pleuritis). There were no irreversible toxicities or treatment-related deaths in this study.

3.3. Efficacy

In level 3, three patients could not start the second course due to haematological toxicities, and in two of the three patients, the response could not be evaluated because of short observation until the start of 2nd line chemotherapy. Among the 26 evaluable patients, eight had a partial response (Table 4). Thus, the overall response was 30.8% (95% confidence

Table 2 – DLTs.

Level	1	2	3
CBDCA (AUC)	5	5	6
S-1 (mg/m^2)	65	80	80
Number of patients	3	3	6
Number of patients with any DLT/Number of patients	0/3	0/3	3/6[a]

a Dose-limiting toxicities, by definition, required a delay in administration of the second course exceeding 14 d. CBDCA, carboplatin; AUC, area under the curve.

Table 3 – Haematological and non-haematological adverse events (n = 28).

Adverse events	1	2	3	4
Haematological toxicity				
Leukocytopaenia	3	4	2	0
Neutrocytopaenia	5	9	0	0
Anaemia	3	5	4	1
Thrombocytopaenia	2	6	7	2
Non-haematological toxicity				
Gastritis	1	0	1	0
Stomatitis	2	1	0	0
Diarrhoea	0	0	0	0
Constipation	4	2	0	0
Anorexia	3	2	1	0
Nausea/vomiting	8	2	1	0
Dysgeusia	2	0	0	0
Fatigue	6	2	1	0
Skin rash	4	1	0	0
T-Bil	1	0	1	0
AST/ALT	1	1	0	0
Infection	0	1	3[a]	0
Febrile neutropaenia	0	0	0	0

a Three cases; two with pneumonitis and one with pleuritis.

interval: 17.1–58.3%) in per protocol sets. In level 2, the recommended dose, among 19 patients, seven had a partial response. The response was 36.8% (95% CI: 16.3–61.6%). One patient treated at level 1 for four cycles had a partial response.

The median follow-up period was 16 months (range, 7–32 months). The median overall survival time was 11.1 months (95% CI: 8.1–15.3 months) and the median progression-free survival time was 5.0 months (95% CI: 3.6–6.0 months) (Fig. 1A and B).

4. Discussion

Systemic chemotherapy for advanced stage NSCLC is regarded as palliative; therefore, the main purpose is to maintain quality of life during an extended survival period. The current standard chemotherapy for stage wet IIIB (a subgroup including patients with malignant effusion and/or no indications for radiation) or stage IV is platinum doublets.[5] Cisplatin combinations confer a survival advantage than carboplatin combinations, according to one meta-analysis[13]; however, the difference was minor. Cisplatin-containing regimens require hospitalisation because massive hydration is essential to preventing renal toxicity, and their use is often restricted by renal, neuropathic and emetogenic toxicities. Although, the combination of carboplatin and paclitaxel is unique and is the most frequently used regimen in the world, among the standard treatments for advanced NSCLC[14], the infusion time remains rather long and additional supportive treatments are needed to prevent allergic reactions.[15] Furthermore, peripheral neurotoxicity is occasionally problematic.

Many reports have suggested synergistic anti-tumour effects when platinum and fluoropyrimidines, including 5FU[16] and S-1[17], are used together. A recent randomised phase III trial in Japan[18] showed a combination of cisplatin with S-1 to be a feasible standard regimen for advanced gastric cancer. The combination of cisplatin and S-1 was also active in patients with NSCLC.[10] Thus, the combination of carboplatin plus S-1 is a potential regimen, possibly shortening hospitalisation as well as being convenient, if it can achieve activity equivalent to those of other standard platinum doublets.

Table 4 – Tumour response.

	Number of patients	Response				
		CR	PR	SD	PD	NE
Part of Phase I						
Level 1	3	0	1	1	1	0
Level 2	3	0	2	1	0	0
Level 3	6	0	0	4	0	2
Part of Phase II						
Level 2	16	0	5	9	2	0
Total	28	0	8	15	3	2

Response rate at the recommended dose: 36.8% (95% CI: 16.3–61.6%).
CR, complete response; PR, partial response; SD, stable disease, PD, progressive disease, NE, not evaluable.
Tumour responses were evaluated using RECIST criteria.

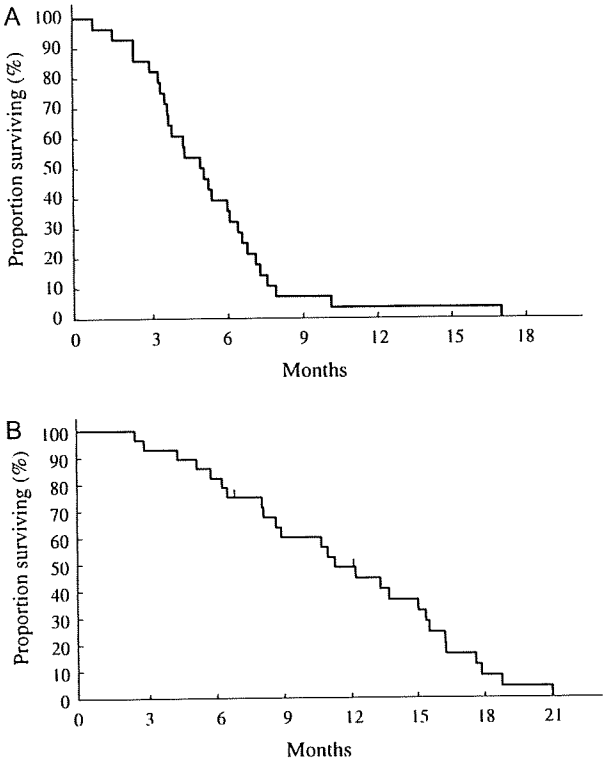

Fig. 1 – (A) Kaplan–Meier curve for progression-free survival (PFS) of all eligible patients (n = 28). Median PFS was 5.0 months (95% CI: 3.6–6.0 months). (B) Kaplan–Meier curve for overall survival. (OS) of all eligible patients (n = 28). Median OS was 11.1 months (95% CI: 8.1–15.3 months).

The RD of the combination was level 2 (AUC5 of CBDCA on day 1 and 80 mg/m^2 of S1 on days 1 to 14, every 3 weeks). This level was not found to be acceptable in a previous report by Kaira et al.[19] despite treatment every 4 weeks. One possible explanation is that they treated only three patients at this level and one was quite elderly, suggesting individual variation. We assessed 19 patients at level 2 in this study, and two (10.5%) had grade 4 thrombocytopaenia, while one (5%) had grade 4 anaemia. No patients experienced febrile neutropaenia, blood transfusion or bleeding, suggesting the safety of level 2. The DLT was the necessity of a delay exceeding 14 d in administration of the second course, due to thrombocytopaenia and neutropaenia, at level 3. However, the median interval until the course at level 2 was 22 (21–44) d, and the median number of treatment cycles was four (range 2–6), suggesting that the treatment schedule could be maintained in most cases. As to haematological toxicity, there were three grade 3 lung infections in two patients, but both recovered with antibiotic treatment were able to resume the chemotherapy. Overall, the incidence of adverse events at the RD appeared to be lower than that with the standard chemotherapy for NSCLC.

The response rate at the RD was 36.8%, i.e. equivalent to those of other standard platinum doublets. The median overall survival time was 11.1 months and the median progression-free survival time was 5.0 months. These rates were not inferior to those of carboplatin/paclitaxel regimens reported in either a western country[5] or Japan.[20]

In summary, to our knowledge, this is the first report on the RD for a carboplatin/S-1 combination administered with a 3-week cycle. Furthermore, its effectiveness in the phase II part of the trial was demonstrated. A randomised non-inferiority phase III trial comparing carboplatin/S-1 with carboplatin/paclitaxel in chemotherapy-naïve patients with NSCLC is currently underway. This combination is also considered to be an alternative therapy for elderly patients and those with poor PS.

Conflict of interest statement

None declared.

Acknowledgements

We wish to thank Toshio Shimizu, Erina Hatashita and Yuki Yamada for data management. This study was not supported by specific grand or sponsors.

REFERENCES

1. Jemal A, Siegel R, Ward E, et al. Cancer statistics, 2008. *CA Cancer J Clin* 2008;58:71–96.
2. Kubota K, Watanabe K, Kunitoh H, et al. Phase III randomized trial of docetaxel plus cisplatin versus vindesine plus cisplatin in patients with stage IV non-small-cell lung cancer: the Japanese Taxotere Lung Cancer Study Group. *J Clin Oncol* 2004;22:254–61.
3. Le Chevalier T, Brisgand D, Douillard JY, et al. Randomised study of vinorelbine and cisplatin versus vindesine and cisplatin versus vinorelbine alone in advanced non-small cell lung cancer: Results of a European multicenter trial including 612 patients. *J Clin Oncol* 1994;12:360–8.
4. Cardenal F, López-Cabrerizo MP, Antón A, et al. Randomized phase III study of gemcitabine-cisplatin versus etoposide-cisplatin in the treatment of locally advanced or metastatic non-small-cell lung cancer. *J Clin Oncol* 1999;17:12–8.
5. Schiller JH, Harrington D, Belani CP, et al. Comparison of four chemotherapy regimens for advanced non-small cell lung cancer. *N Engl J Med* 2002;346:92–8.
6. Shirasaka T, Shimamoto Y, Ohshimo H, et al. Department of a novel form of an oral 5-fluorouracil derivative (S-1) directed to the potentiation of the tumor selective cytotoxicity of 5-fluorouracil by two biochemical modulators. *Anticancer Drugs* 1996;7:548–57.
7. Takechi T, Fujioka A, Matsushima E, Fukushima M. Enhancement of the antitumour activity of 5-fluorouracil (5-FU) by inhibiting dihydropyrimidine dehydrogenase activity (DPD) using 5-chloro-2, 4-dihydroxypyridine (CDHP) in human tumour cells. *Eur J Cancer* 2002;38:1271–7.
8. Takechi T, Nakano K, Uchida J, et al. Antitumor activity and low intestinal toxicity of S-1, a new formulation of oral tegafur, in experimental tumor models in rats. *Cancer Chemother Pharmacol* 1997;39:205–11.
9. Kawahara M, Furuse K, Segawa Y, et al. Phase II study of S-1, a novel oral fluorouracil, in advanced non-small-cell lung cancer. *Br J Cancer* 2001;85:939–43.

10. Ichinose Y, Yoshimori K, Sakai H, et al. S-1 plus cisplatin combination chemotherapy in patients with advanced non-small cell lung cancer: a multi-institutional phase II trial. *Clin Cancer Res* 2004;10:7860–4.
11. Calvert AH, Newell DR, Gumbrell LA, et al. Carboplatin dosage: prospective evaluation of a simple formula based on renal function. *J Clin Oncol* 1989;7:1748–56.
12. Therasse P, Arbuck SG, Eisenhauer EA, et al. New guidelines to evaluate the response to treatment in solid tumors. *J Natl Cancer Inst* 2000;92:205–16.
13. Hotta K, Matsuo K, Ueoka H, et al. Meta-analysis of randomized clinical trials comparing Cisplatin to Carboplatin in patients with advanced non-small-cell lung cancer. *J Clin Oncol* 2004;22:3852–9.
14. Socinski MA, Crowell R, Hensing TE, et al. Treatment of non-small cell lung cancer, stage IV: ACCP evidence-based clinical practice guidelines (2nd edition). *Chest* 2007;132(Suppl. 3): 277S–289S.
15. Weiss RB, Donehower RC, Wiernik PH, et al. Hypersensitivity reactions from taxol. *J Clin Oncol* 1990;8:1263–8.
16. Shirasaka T, Shimamoto Y, Ohshimo H, et al. Metabolic basis of the synergistic antitumor activities of 5-fluorouracil and cisplatin in rodent tumor models in vivo. *Cancer Chemother Pharmacol* 1993;32:167–72.
17. Sakaki E, Tominaga K, Kuwamura H, et al. Synergistic antitumor effect of combined 5-fluorouracil (5-FU) with 5-chloro-2, 4-dihydroxypyridine on 5-FU-resistant gastric cancer cells: possible role of a dihydropyrimidine dehydrogenase-independent mechanism. *J Gastroenterol* 2007;4:816–22.
18. Koizumi W, Narahara H, Hara T, et al. S-1 plus cisplatin versus S-1 alone for first-line treatment of advanced gastric cancer (SPIRITS trial): a phase III trial. *Lancet Oncol* 2008;9:215–21.
19. Kaira K, Sunaga N, Yanagitani N, et al. A phase I dose-escalation study of S-1 plus carboplatin in patients with advanced non-small-cell lung cancer. *Anticancer Drugs* 2007;18:471–6.
20. Ohe Y, Ohashi Y, Kubota K, et al. Randomized phase III study of cisplatin plus irinotecan versus carboplatin plus paclitaxel, cisplatin plus gemcitabine, and cisplatin plus vinorelbine for advanced non-small-cell lung cancer: Four-Arm Cooperative Study in Japan. *Ann Oncol* 2007;18:317–23.

Oncogene (2009) 28, 518–533

www.nature.com/onc

ORIGINAL ARTICLE

Disruption of the EGFR E884–R958 ion pair conserved in the human kinome differentially alters signaling and inhibitor sensitivity

Z Tang[1], S Jiang[1], R Du[1], ET Petri[2], A El-Telbany[1], PSO Chan[3], T Kijima[4], S Dietrich[1], K Matsui[5], M Kobayashi[5], S Sasada[5], N Okamoto[5], H Suzuki[5], K Kawahara[6], T Iwasaki[7], K Nakagawa[7], I Kawase[4], JG Christensen[8], T Hirashima[5], B Halmos[1], R Salgia[9], TJ Boggon[2], JA Kern[10] and PC Ma[1]

[1]*Division of Hematology/Oncology, Case Western Reserve University School of Medicine, University Hospitals Case Medical Center and Ireland Cancer Center, Case Comprehensive Cancer Center, Cleveland, OH, USA;* [2]*Department of Pharmacology, Yale University School of Medicine, New Haven, CT, USA;* [3]*Elpidex Bioscience Inc., Los Angeles, CA, USA;* [4]*Department of Respiratory Medicine, Allergy and Rheumatic Diseases, Osaka University Graduate School of Medicine, Osaka, Japan;* [5]*Department of Thoracic Malignancy, Osaka Prefectural Medical Center for Respiratory and Allergic Disease, Osaka, Japan;* [6]*Department of Pathology, Osaka Prefectural Medical Center for Respiratory and Allergic Disease, Osaka, Japan;* [7]*Department of Thoracic Surgery, Osaka Prefectural Medical Center for Respiratory and Allergic Disease, Osaka, Japan;* [8]*Pfizer Inc., Global Research and Development, San Diego, CA, USA;* [9]*Section of Hematology/Oncology, University of Chicago Pritzker School of Medicine, University of Chicago Cancer Research Center, Chicago, IL, USA and* [10]*Division of Pulmonary, Critical Care and Sleep Medicine, Case Western Reserve University School of Medicine, University Hospitals Case Medical Center and Ireland Cancer Center, Case Comprehensive Cancer Center, Cleveland, OH, USA*

Targeted therapy against epidermal growth factor receptor (EGFR) represents a major therapeutic advance in lung cancer treatment. Somatic mutations of the *EGFR* gene, most commonly L858R (exon 21) and short in-frame exon 19 deletions, have been found to confer enhanced sensitivity toward the inhibitors gefitinib and erlotinib. We have recently identified an EGFR mutation E884K, in combination with L858R, in a patient with advanced lung cancer who progressed on erlotinib maintenance therapy, and subsequently had leptomeningeal metastases that responded to gefitinib. The somatic E884K substitution appears to be relatively infrequent and resulted in a mutant lysine residue that disrupts an ion pair with residue R958 in the EGFR kinase domain C-lobe, an interaction that is highly conserved within the human kinome as demonstrated by our sequence analysis and structure analysis. Our studies here, using COS-7 transfection model system, show that E884K works in concert with L858R in-*cis*, in a dominant manner, to change downstream signaling, differentially induce Mitogen-activated protein kinase (extracellular signaling-regulated kinase 1/2) signaling and associated cell proliferation and differentially alter sensitivity of EGFR phosphorylation inhibition by ERBB family inhibitors in an inhibitor-specific manner. Mutations of the conserved ion pair E884–R958 may result in conformational changes that alter kinase substrate recognition. The analogous E1271K-MET mutation conferred differential sensitivity toward preclinical MET inhibitors SU11274 (unchanged) and PHA665752 (more sensitive). Systematic bioinformatics analysis of the mutation catalog in the human kinome revealed the presence of cancer-associated mutations involving the conserved E884 homologous residue, and adjacent residues at the ion pair, in known proto-oncogenes (*KIT*, *RET*, *MET* and *FAK*) and tumor-suppressor gene (*LKB1*). Targeted therapy using small-molecule inhibitors should take into account potential cooperative effects of multiple kinase mutations, and their specific effects on downstream signaling and inhibitor sensitivity. Improved efficacy of targeted kinase inhibitors may be achieved by targeting the dominant activating mutations present.
Oncogene (2009) **28,** 518–533; doi:10.1038/onc.2008.411; published online 17 November 2008

Keywords: *EGFR*; *MET*; mutation; tyrosine kinase inhibitor; structure; kinome

Correspondence: Dr PC Ma, Division of Hematology/Oncology, Case Western Reserve University School of Medicine, University Hospitals Case Medical Center and Ireland Cancer Center, Case Comprehensive Cancer Center, 10900 Euclid Avenue, WRB 2-123, Cleveland, OH 44106, USA.
E-mail: patrick.ma@case.edu
Received 10 March 2008; revised 17 September 2008; accepted 1 October 2008; published online 17 November 2008

Introduction

Targeted therapy using epidermal growth factor receptor (EGFR) kinase inhibitors represents a major therapeutic advance in lung cancer treatment. Somatic mutations of the *EGFR* gene, most commonly L858R (exon 21) and short in-frame deletions in exon 19, have recently been identified as catalytic domain mutation hotspots (Shigematsu and Gazdar, 2006). These mutations confer enhanced sensitivity toward the anilinoquinazoline kinase inhibitors gefitinib and erlotinib (Lynch *et al.*, 2004;

Paez *et al.*, 2004). A mutation conferring resistance to these two kinase inhibitors, T790M (exon 20), has also been found in the EGFR kinase domain and can account for about half of the cases of acquired resistance (Kobayashi *et al.*, 2005). There are a number of other kinase domain mutations of EGFR that occur at lower frequencies, most often in combination with L858R (Tam *et al.*, 2006). However, how these mutations might interact when present together in-*cis* is unknown.

We recently identified a novel EGFR kinase domain somatic mutation, E884K (Glu884Lys, exon 22) in a patient with stage IV non-small-cell lung cancer, in combination with the L858R mutation (L858R + E884K) (Choong *et al.*, 2006). The patient initially received carboplatin/paclitaxel and erlotinib and then developed brain metastasis on maintenance erlotinib. In spite of further treatment with whole brain radiation, temozolomide and irinotecan, the patient's disease progressed to symptomatic leptomeningeal carcinomatosis, which responded to gefitinib, a year after being off an EGFR kinase inhibitor. The L858R + E884K double mutation was found both in her pretreatment diagnostic thoracic lymph node biopsy specimen as well as in the tumor cells (extracted by laser microdissection) within the cerebrospinal fluid during the course of leptomeningeal metastases (Choong *et al.*, 2006). The E884K mutation represents the first mutation reported to show an apparent differential response to the two EGFR kinase inhibitors erlotinib and gefitinib, whereas L858R was known to be sensitizing to both. These findings led to our hypothesis that EGFR kinase mutations can work together to differentially alter inhibitor sensitivity and downstream signaling. Further biochemical analysis in our current study indicates that the double mutant EGFR (L858R + E884K) responds differently to gefitinib and erlotinib. We now show that E884K works in concert with L858R, and in a dominant manner, to mediate differential sensitivity to kinase inhibitors through altered phosphorylation of AKT and signal transducer and activator of transcription 3 (STAT3) and were correlated with differential cellular cytotoxicity and induction of the apoptotic marker cleaved-PARP(Asp214) by EGFR inhibitors. Using a combination of bioinformatics and structural analyses, we further characterized the role of the E884 residue in EGFR kinase function. Our results further demonstrate that the ion pair formed by residues E884 and R958 in the EGFR kinase domain is a highly conserved feature of protein kinases in the human kinome, including many 'druggable' targets such as MET. Disruption of the conserved ion pair in EGFR modulates downstream signal transduction and differentially alters kinase inhibitor sensitivity in an inhibitor-specific manner.

Results

E884K works in concert with L858R mutation to confer differential inhibitor sensitivity through inhibition of AKT and STAT3 downstream signaling

We hypothesize that EGFR kinase mutations can work together to differentially alter inhibitor sensitivity. To test this hypothesis, *EGFR* expression constructs engineered with L858R (LR) or dual mutations of L858R + E884K (LR + EK) were stably transfected into COS-7 cells. Cells were treated with increasing concentrations of either erlotinib or gefitinib in the presence of EGF stimulation (Figure 1a). Compared with L858R alone, the L858R + E884K dual mutant was less sensitive to erlotinib in the inhibition of tyrosine phosphorylation of EGFR. Conversely, E884K worked in concert with L858R in-*cis* to further enhance the sensitivity of the mutant receptor to gefitinib inhibition (Figures 1a and b). These findings correlated with the clinical course of the patient's response profile (Choong *et al.*, 2006) and highlight the potential for EGFR kinase mutations to exert concerted effects in-*cis* to impact targeted inhibition.

To gain insight into the mechanism of E884K modulation of EGFR tyrosine kinase inhibitor (TKI) sensitivity, we further studied its effect on downstream AKT and STAT3 signaling pathways with TKI inhibition. The effect on the downstream signal mediators p-AKT (S473) and p-STAT3 (Y705) correlated well with the inhibition of EGFR phosphorylation (Figure 1a); E884K in-*cis* with L858R decreased erlotinib inhibition of AKT and STAT3 phosphorylation but increased inhibition by gefitinib. The differential inhibition exerted by E884K on EGFR, AKT and STAT3 signaling also corresponded to the inhibitor-induced expression pattern of the apoptotic marker, cleaved-PARP(Asp214) (Figure 1c). Similarly, there was an opposite effect of the E884K mutation over L858R in-*cis* in inducing cellular cytotoxicity by erlotinib and gefitinib (Figure 1d). Hence, E884K in-*cis* with L858R differentially altered inhibitor sensitivity when compared with L858R alone, through differential inhibition of the prosurvival AKT and STAT3 signaling pathways associated with altered induction of cleaved-PARP(Asp214).

E884K-EGFR modulates inhibitor sensitivity effects in an inhibitor-specific manner

To further examine the hypothesis that EGFR mutations exert effects in combination that are unique to a specific kinase inhibitor, we further tested the mutant EGFR expressing L858R alone or L858R + E884K in-*cis*, against several other ERBB family TKIs, including both reversible inhibitors (4557W, Lapatinib, GW583340, Tyrphostin-AG1478) and irreversible inhibitor (CL-387,785) (Figure 2 and Supplementary Figure 2). We focused on the effects of these inhibitors on the sensitivity of inhibition of the EGFR kinase phosphorylation in the mutant EGFR. As the tyrosine phosphorylation of the EGFR has been shown to correlate well with its catalytic enzymatic activity, we used the tyrosine phosphorylation of the pY1068 (GRB1-binding site) epitope of EGFR as the surrogate measurement of the extent of inhibition by the TKIs. For 4557W (reversible dual TKI of EGFR/ERBB2), the E884K mutation modulated the L858R mutation in-*cis*, again in a dominant manner, rendering the double-mutant receptor more sensitive to the dual inhibitor

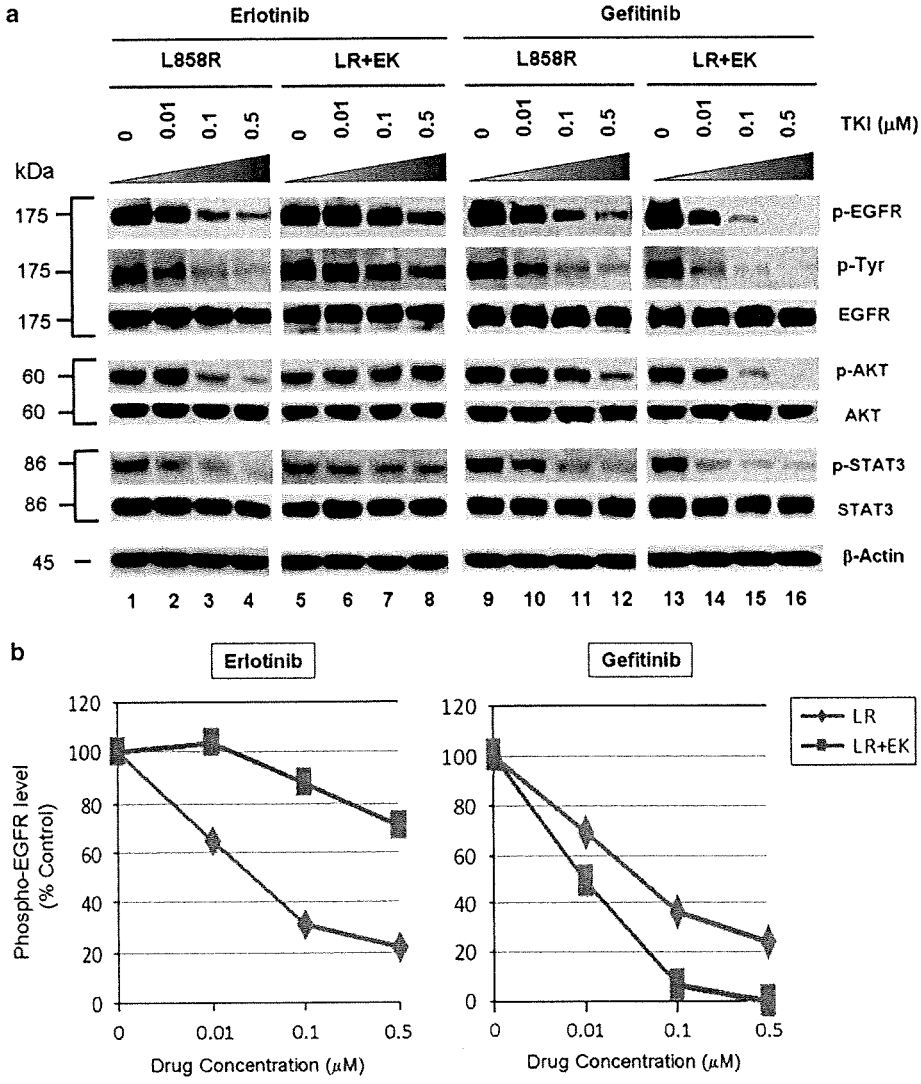

Figure 1 E884K mutation of epidermal growth factor receptor (EGFR) worked in concert with L858R to differentially alter sensitivity to EGFR kinase inhibitors erlotinib and gefitinib. (**a**) Stable COS-7 transfects expressing the L858R and double-mutant L858R + E884K variants of *EGFR* were used in the experiment. The endogenous wild-type EGFR expression of parental COS-7 cells is negligible (data not shown). Cells were cultured in 0.5% bovine serum albumin-containing serum-free media for 16 h and then incubated with increasing concentrations of either erlotinib or gefitinib in the presence of EGF (100 ng/ml). Whole-cell lysates were extracted for SDS–polyacrylamide gel electrophoresis and immunoblotting using antibodies against: p-EGFR (Y1068), phosphotyrosine (p-Tyr), EGFR, p-AKT (S473), AKT, p-STAT3 (Y705), STAT3 and β-actin. The experiment was performed in duplicate with reproducible results. The E884K mutation negatively modulated the effect of L858R to erlotinib inhibition in a dominant manner but enhanced sensitivity of the mutant receptor to gefitinib inhibition. (**b**) Densitometric quantitation of the p-EGFR (Y1068) levels showing differential alteration of sensitivity to erlotinib (more resistant) and gefitinib (more sensitive) by the E884K mutation when in-*cis* with L858R. The densitometric scanning of the p-EGFR immunoblot bands was performed digitally using the NIH ImageJ software program and was normalized to the total EGFR expression levels. (**c**) Relative expression of the apoptotic marker cleaved-PARP(Asp214) in L858R and L858R + E884K *EGFR* variants treated with increasing concentrations of erlotinib (left) and gefitinib (right). The immunoblot from whole cell lysates as in (**a**), using anti-cleaved-PARP(Asp214) (c-PARP) antibody is shown here (above) together with the densitometric quantitation (below) adjusted to β-actin loading control using the NIH ImageJ software program. (**d**) COS-7 cells with stable transduced expression of L858R or L858R + E884K mutant *EGFR* were tested in cellular cytotoxicity assay *in vitro* under drug treatment with either erlotinib or gefitinib at indicated concentrations. Results are shown in percentage change of cell viability of L858R + E884K EGFR-COS-7 compared with the control L858R EGFR-COS-7 cells at each concentration of TKI tested. E884K mutation, when in-*cis* with L858R, significantly decreased the sensitivity of cell viability inhibition by erlotinib compared with L858R alone; however, it significantly increased the sensitivity of cell viability inhibition by gefitinib compared with L858R alone. In the case of erlotinib, E884K was desensitizing to L858R, leading to lower cytotoxicity (56.3 ± 2.68% increased viable cells after inhibition at 5 μM, $P = 0.0004$) compared with L858R alone. Conversely, in gefitinib inhibition, E884K further sensitized L858R in-*cis*, leading to significantly higher cytotoxicity (63.5 ± 6.86% decreased viable cells after inhibition at 5 μM, $P = 0.0013$) compared with L858R alone. Error bar, s.d. ($N = 3$). $^*P < 0.05$, compared with L858R alone. Representative photomicrographs of cells after 48 h of indicated inhibitor treatment (5 μM) *in vitro* were included to illustrate the presence of differential cytotoxicity as seen with the nonviable detached cells or cell fragments (× 10). Examples of increased floating nonviable cells are highlighted with arrows.

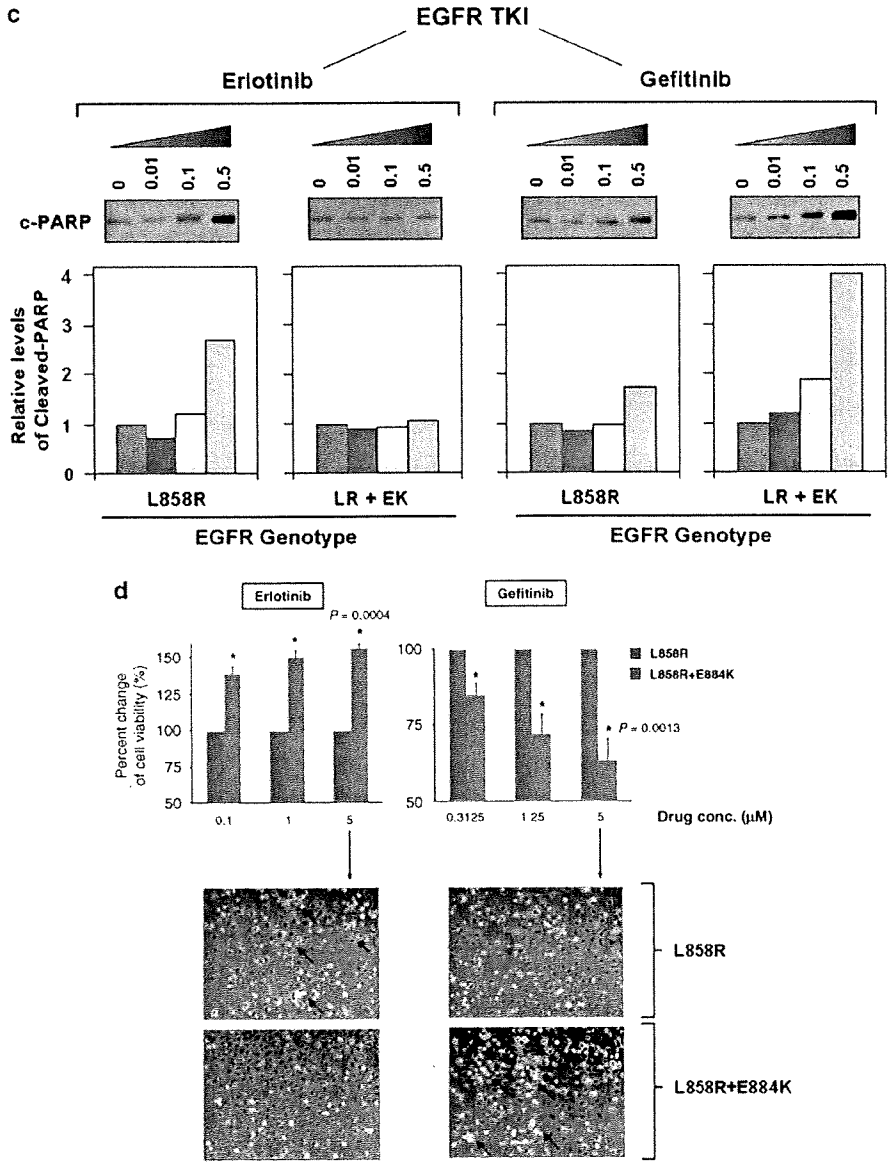

Figure 1 Continued.

(Figure 2). Hence, E884K mutation can work in concert with L858R to modulate mutant receptor sensitivity to different targeted inhibitors. Similarly, E884K further enhanced the sensitivity of L858R to the inhibition by the irreversible EGFR/ERBB2 inhibitor, CL-387,785. On the other hand, the sensitivity of EGFR phosphorylation between the L858R and L858R + E884K EGFR receptors in Tyrphostin-AG1478 (reversible EGFR-TKI), GW583340 (reversible dual EGFR/ERBB2-TKI) and lapatinib (reversible dual EGFR/ERBB2-TKI) did not significantly differ. Hence, the E884K mutation, when in-*cis* with L858R, modulates the sensitivity of the mutant receptor toward ERBB family kinase inhibitors in an inhibitor-specific manner.

E884K is activating, and can work cooperatively with L858R to differentially modulate downstream signal transduction

To address the question whether there are other downstream phosphoproteins that can be differentially activated by the E884K mutation compared with the activating L858R mutation, the global phosphotyrosine profiles of the cellular proteins induced by the mutant EGFR were examined. The E884K alone and L858R + E884K double-mutant EGFR remained sensitive to EGF, and the E884K mutation cooperates with L858R when in-*cis* to further enhance the mutational effects on downstream phosphoprotein activation (data not shown). To date, essentially all mutational combinations involving L858R studied thus far were found to

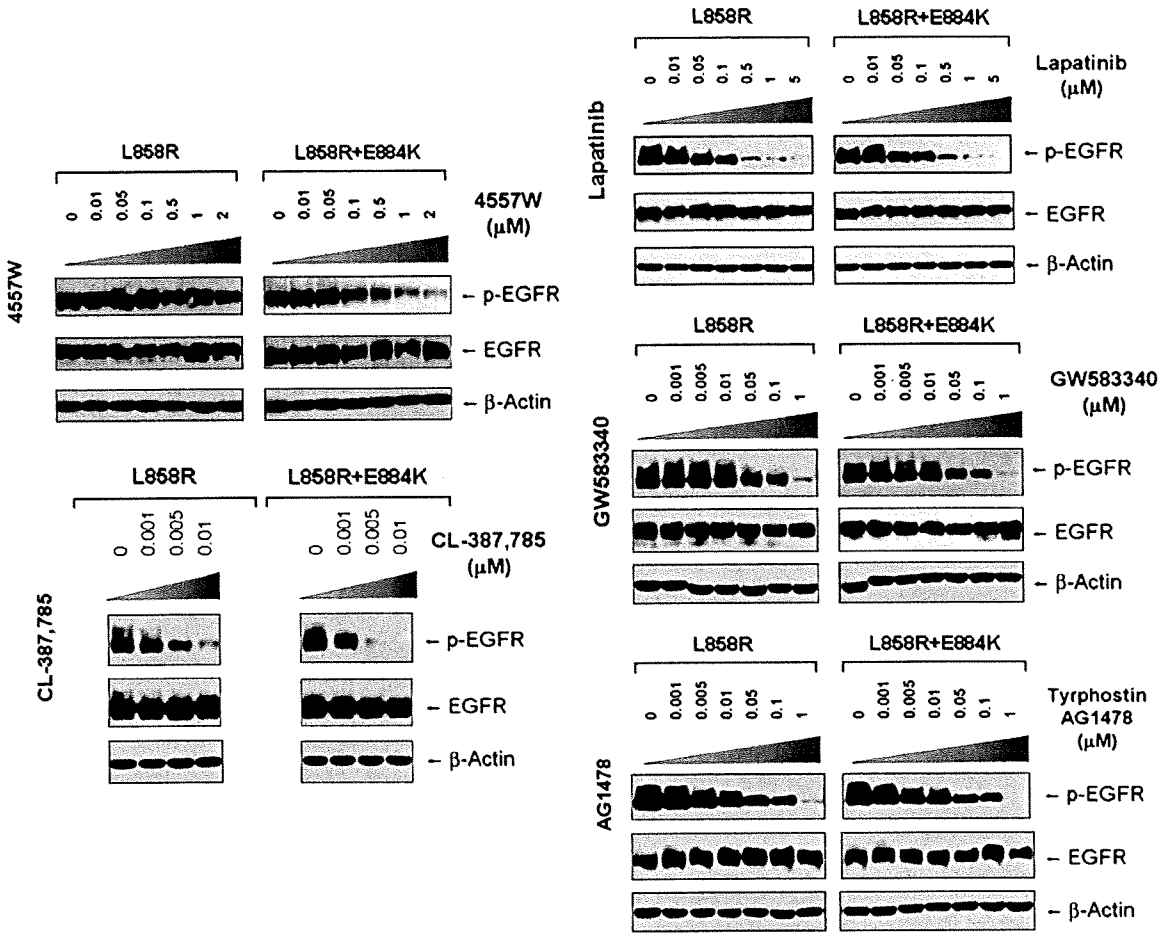

Figure 2 Effects of L858R/E884K-EGFR on other epidermal growth factor receptor (EGFR) kinase inhibitors. The EGFR mutation E884K modulated L858R mutation in-*cis* with inhibitor-specific effects on the sensitivities to EGFR phosphorylation inhibition by the inhibitors (4557W, GW583340, Tyrphostin-AG1478, lapatinib and CL-387,785). Stable COS-7 transfectant cells expressing equivalent levels of the following *EGFR* variants were used: L858R (LR) and L858R + E994K (LR + EK). Cells were cultured in 0.5% bovine serum albumin-containing serum-free media for 16 h, and then treated with or without increasing concentrations of the EGFR TKIs as indicated, in the presence of EGF stimulation (100 ng/ml). Whole cell lysates were extracted for SDS–polyacrylamide gel electrophoresis and immunoblotting using the following antibodies: p-EGFR (Y1068), EGFR and β-actin. E884K mutation worked in concert with L858R in-*cis* to enhance the sensitivity of the mutant receptor to inhibition by the kinase inhibitor 4557W, and CL-387,785. On the other hand, it has little effects on the inhibition by lapatinib, GW583340 and Tyrphostin-AG1478.

exist in-*cis*, suggesting potential *cis* mutation-to-mutation cooperation in EGFR signaling and possibly tumorigenesis (Tam *et al.*, 2006). To determine the effect of E884K on mutant EGFR signaling, we next studied the EGFR activation of the downstream PI3K-AKT-MAPK (ERK1/2)-STAT pathway. E884K mutant (alone or in-*cis* with L858R) receptor exhibited constitutive activation of the tyrosine phosphorylated EGFR comparable with L858R (Figure 3a). E884K and L858R + E884K mutants remained sensitive to EGF and were activated by the ligand to a level comparable with L858R (Figure 3a). L858R was associated with downstream activation of p-AKT signaling, which was inducible by EGF stimulation. When in-*cis* with L858R, E884K mutation (L858R + E884K) downregulated constitutive AKT phosphorylation. E884K, alone or in-*cis* with L858R, can also mediate constitutive induction of p-STAT3 (pY705) (important for STAT3 dimerization and transcriptional activation of target genes) (Figure 3a). Interestingly, the double mutation L858R + E884K conferred a distinctly more sensitive response to EGF stimulation selectively in the mitogen-activated protein kinase (extracellular signaling-regulated kinase 1/2) (MAPK-ERK1/2) cell proliferation pathway compared with either wild type, E884K alone or L858R alone. Consistent with this differential signaling effect, the L858R + E884K-COS-7 cells had a significantly higher cell proliferation rate than that of the L858R-COS-7 cells in the MTS cell proliferation assay for 5 days (Figure 3b). At days 3 and 5, the cell proliferation rate as determined by % viable cell increase during the assay period was 1.46-fold (day 3) and 1.40-fold ($P = 0.0013$) higher (day 5) in L858R + E884K than L858R alone. L858R + E884K

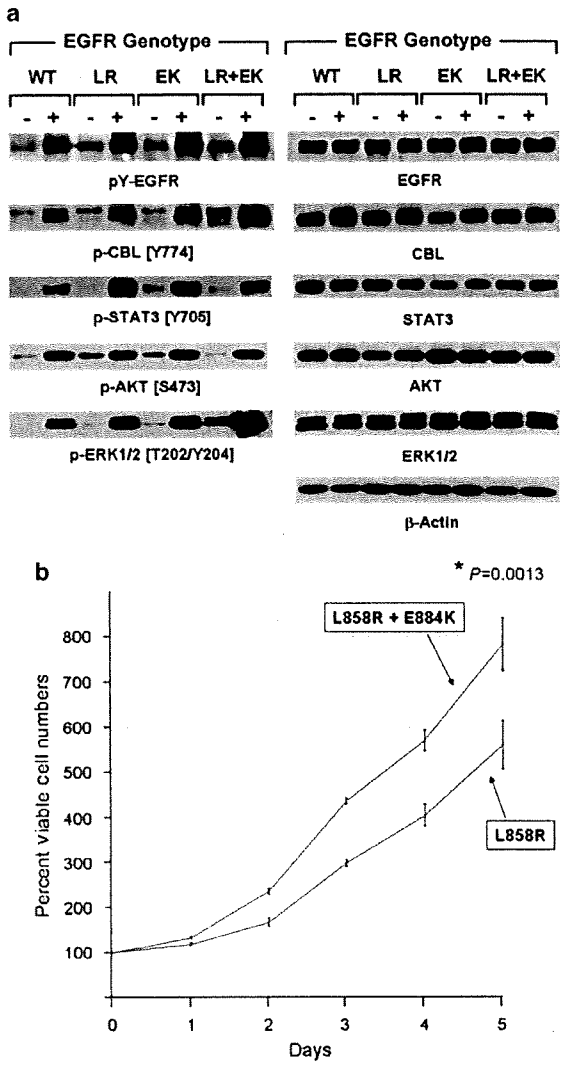

Figure 3 Effects of mutational disruption of the Glu(E)884–Arg(R)958 ion pair in epidermal growth factor receptor (EGFR) signaling. (**a**) Stable COS-7 transfectant cells expressing the various *EGFR* variants were cultured in 0.5% bovine serum albumin-containing serum-free media, followed by EGF stimulation (100 ng/ml, 10 min). Whole cell lysates were prepared for SDS–polyacrylamide gel electrophoresis and immunoblotted using the antibodies against: phosphotyrosine (pY-EGFR), EGFR, p-CBL (Y774), CBL, p-STAT3 (Y705), STAT3, p-AKT (S473), AKT, p-ERK1/2 (T202/Y204), ERK1/2 and β-actin. E884K, either alone or in-*cis* with L858R, modulated differential activation of downstream mutant EGFR signaling. (**b**) The EGFR double mutations L858R + E884K conferred a significantly higher cell proliferation rate than L858R alone in the COS-7 cells stably expressing the transduced mutant *EGFR*. Cellular viability assay was performed with the cells growing in regular growth media (10% fetal bovine serum) up to 5 days as described in Materials and methods. The MTS viability assay was performed in triplicate. Error bar, s.d. $^*P = 0.0013$.

also conferred a higher induction of p-CBL as well. Hence, the double mutation L858R + E884K modulated basal and stimulated downstream EGFR signaling differentially with differential effects on the AKT (downregulated), CBL and MAPK-ERK1/2 phosphorylation (upregulated). Moreover, E884K had a dominant effect over L858R, when in-*cis*, in these signaling modulatory effects.

Disruption of a conserved ion pair, Glu(E)884-Arg(R)958, in EGFR differentially alters kinase inhibitor sensitivity

Next, bioinformatics analysis of the E884 residue was performed by multiple kinase domain amino-acid sequence alignments of the human kinome, using the AliBee multiple sequence alignment program (GeneBee, Moscow, Russia) (Supplementary Figure 1). Amino-acid alignments of the kinase domains of phylogenetically diverse groups of kinases such as among the ERBB family, the vascular endothelial growth factor receptor family and the TRK family show that the E884 residue is highly conserved (Figure 4a). In addition, a second residue was also found to be highly conserved (R958) (Figure 4a). Further multiple sequence alignments of 321 human kinase domains show high conservation of both E884 and R958 residues of the EGFR kinase domain (Supplementary Figure 1). The glutamic acid residue (E884) is conserved in > 77% and the arginine residue (R958) is conserved in > 55% of human kinases in the kinome.

Finally, we mapped the locations of the L858R and E884K mutations onto the three-dimensional structure of the EGFR kinase domain complexed with erlotinib and with lapatinib (PDB accession codes 1M17 (Stamos *et al*., 2002) and 1XKK (Wood *et al*., 2004)) (Figure 4b). We also generated a superposition of the EGFR kinase domain with multiple diverse kinase catalytic domains (Figure 4c). These analyses show the structural conservation of the buried Glu(E)-Arg(R) ion pair and that the exon 22 residue, E884, is physically distant from L858 in exon 21. Furthermore, unlike L858, E884 is not proximal to the adenosine triphosphate-binding cleft of the kinase domain, making it difficult to predict its effects on kinase inhibitor interactions. Mutation of the acidic glutamate residue at codon 884 to a basic lysine will disrupt the highly conserved ion pair through charge–charge repulsion with the basic residue R958 (Figures 4b and c).

To further test the hypothesis of the disruption of the conserved E884–R958 salt bridge as a mechanism underlying the differential response of the mutant EGFR to kinase inhibitors, we tested the double mutant L858R + R958D against erlotinib and gefitinib (Figure 5). Substitution of the wild-type Arg(R)958 with Asp(D)958 was created using site-directed mutagenesis. We hypothesized that the R958D substitution would disrupt the ion pair with E884 through electrostatic repulsion, in a way similar to the effect of the E884K substitution. COS-7 cells transfected to express the indicated mutant EGFR receptors were inhibited using either erlotinib or gefitinib *in vitro* with increasing concentrations. Similar to E884K, R958D modulated the sensitizing effect of L858R differentially to reversible EGFR inhibitors when in-*cis* (with L858R). R958D mutation, when in-*cis* with L858R, decreased the

sensitivity of the mutant receptor to erlotinib inhibition, while increasing the sensitivity to gefitinib in a dominant manner (Figures 5a and b).

Mutational disruption of the conserved kinase ion pair in MET kinase by E1271K-MET also differentially alters the sensitivity of phosphorylation inhibition by MET inhibitors

MET has been shown to play a key role in the development of many human malignancies. A number of mutations have been identified in *MET* from various cancers. Recently, it has been shown that MET represents a key oncogenic signaling in lung cancer alongside with EGFR signaling (Rikova *et al.*, 2007; Guo *et al.*, 2008; Tang *et al.*, 2008). Moreover, MET can cross-activate with EGFR when they are co-expressed, which happens rather frequently (Rikova *et al.*, 2007; Tang *et al.*, 2008). MET has also been shown to be an attractive therapeutic molecular target (Ma *et al.*, 2003b; Shinomiya *et al.*, 2004; Mazzone and Comoglio, 2006; Peruzzi and Bottaro, 2006; Smolen *et al.*, 2006). Here, we test the hypothesis that E1271K mutation of *MET*, analogous to E884K-*EGFR*, can also differentially alter inhibitory sensitivity toward selective MET inhibitors (Figure 6). The Glu(E)1271-Arg(R)1345 constitutes the conversed ion-pair in MET kinase (Figures 4 and 6). The location of the E1271–R1234 ion pair in MET kinase is illustrated in the recently reported crystallographic structure of the MET kinase domain complexed with SU11274 (Bellon *et al.*,

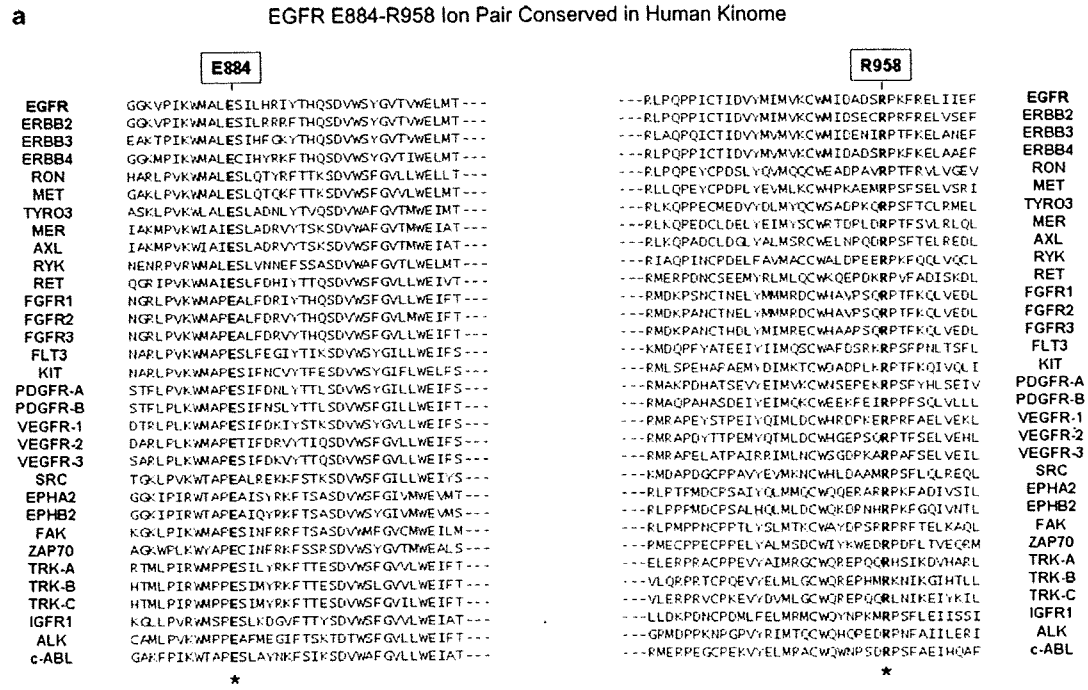

Figure 4 The ion pair Glu(E)884-Arg(R)958 in the epidermal growth factor receptor (EGFR) kinase domain is a highly conserved feature in the human kinome. **(a)** A selected list of 32 diverse human protein kinases with known importance as validated or potential cancer therapeutic targets was included here with bioinformatics alignment analysis of the kinase domain amino-acid sequences. Glu884 (E884) and Arg958 (R958) of EGFR are both highly conserved residues among these kinases. (Left) Amino-acid alignment of the kinase domains of 32 diverse members of human protein kinases showing E884-EGFR is highly conserved: EGFR, ERBB2, ERBB3, ERBB4, RON, MET, TYRO3, MER, AXL, RYK, RET, FGFR1, FGFR2, FGFR3, FLT3, KIT, PDGFR-A, PDGFR-B, vascular endothelial growth factor receptor-1, vascular endothelial growth factor receptor-2, vascular endothelial growth factor receptor-3, SRC, EPHA2, EPHB2, FAK, ZAP70, TRK-A, TRK-B, TRK-C, IGFR1, ALK and c-ABL. (Right) R958-EGFR is also highly conserved among diverse members of kinases. For the complete alignment analysis of kinase domains of the human kinome, see Supplementary Figure 1. **(b)** EGFR kinase domain crystal structures (PDB accession codes 1M17 (Stamos *et al.*, 2002) and 1XKK (Wood *et al.*, 2004)) when in complex with erlotinib (blue) and lapatinib (green) are shown. The locations of L858 (exon 21) and E884 (exon 22) are highlighted. E884 (acidic) and R958 (basic) residues form an ion pair in wild-type EGFR that would be disrupted by the E884K substitution from the acidic glutamic acid (E) to the basic lysine (K). The E884–R958 salt bridge is present in the kinase domain crystal structures complexed to either erlotinib or lapatinib. **(c)** Superposition of the EGFR kinase domain with the catalytic domains of diverse kinases shows structural conservation of a buried Glu(E)–Arg(R) ion pair. The crystal structure of EGFR tyrosine kinase (PDB accession code: 1M17) (Stamos *et al.*, 2002) was superimposed with the catalytic kinase domains of human CDK2 (PDB accession code: 1VYW) (Pevarello *et al.*, 2004), human JNK3 (PDB accession code: 1PMQ) (Scapin *et al.*, 2003), human insulin receptor kinase (PDB accession code: 1IR3) (Hubbard, 1997), ZAP-70 tyrosine kinase (PDB accession code: 1U59) (Jin *et al.*, 2004), LCK kinase (PDB accession code: 1QPD) (Zhu *et al.*, 1999) and MET (PDB accession code: 2RFS) (Bellon *et al.*, 2008) using Cα atoms in the program DeepView/Swiss-PdbViewer v3.7. The conserved Glu–Arg ion pair is shown in stick format, with oxygen atoms colored red and nitrogens, blue. The EGFR side chains are shown in yellow. The structural location of the ion pair is conserved in these crystal structures and helps orientate helix αEF. Figures 4b and c were prepared using the program PYMOL (www.pymol.org).